Widely tunable (2.6–10.4 μm) $BaGa_4Se_7$ optical parametric oscillator pumped by a Q-switched $Nd:YLiF_4$ laser

Journal of Physics Communications

PAPER

Widely tunable (2.6–10.4 μm) $BaGa_4Se_7$ optical parametric oscillator pumped by a Q-switched Nd:$YLiF_4$ laser

D B Kolker[2,3,4], N Yu Kostyukova[1,2], A A Boyko[1,2], V V Badikov[5], D V Badikov[5], A G Shadrintseva[1], N N Tretyakova[1], K G Zenov[1], A A Karapuzikov[1] and J-J Zondy[6]

[1] Special Technologies, Ltd, 1/3 Zeljonaja gorka str., 630060 Novosibirsk, Russia
[2] Research Laboratory of Quantum Optics Technology, Novosibirsk State University, 2 Pirogova Str., 630090 Novosibirsk, Russia
[3] Institute of Laser Physics SB RAS, Lavrentyev av. 13/3, 630090 Novosibirsk, Russia
[4] Novosibirsk State Technical University, K. Marx av. 20, 630073 Novosibirsk, Russia
[5] High Technologies Laboratory, Kuban State University, 149 Stavropolskaya Str., 350040 Krasnodar, Russia
[6] School of Science and Technology, Nazarbayev University, 53 Kabanbay Batyr Ave., 010000 Astana, Kazakhstan

E-mail: dkolker@mail.ru

Keywords: nonlinear chalcogenide ($BaGa_4Se_7$), optical parametric oscillator (OPO), mid-infrared (mid-IR)

OPEN ACCESS

RECEIVED
13 November 2017

REVISED
22 January 2018

ACCEPTED FOR PUBLICATION
16 February 2018

PUBLISHED
22 March 2018

Abstract

We report on the first $BaGa_4Se_7$ nanosecond optical parametric oscillator pumped by Q-switched Nd:$YLiF_4$ laser at 1053 nm. The oscillator exhibits a pump threshold energy as low as 0.25 mJ. Mid-infrared (MIR) idler wave tuning from 2.6 μm to 10.4 μm is demonstrated with an angle-tuned type-I (*o-ee*) *y*-cut sample, highlighting the superior performance of this novel large bandgap chalcogenide nonlinear crystal to generate tunable coherent radiation over its full MIR transparency range (0.47–18 μm). The phase-matching data are used to identify the most accurate dispersion relations of this compound among three recently published Sellmeier equations. Damage threshold measurements yielded values as high as 2.04 J cm^{-2} at 100 Hz pulse repetition rate, one of the largest among existing MIR $\chi^{(2)}$nonlinear materials.

1. Introduction

Widely tunable optical parametric oscillators are attractive laser sources for mid-infrared (MIR) nonlinear optics applications, because of the scarcity of direct-emitting conventional laser sources in this spectral region (2–20 μm). While oxide-based periodically-poled nonlinear compounds belonging to the ferroelectric crystal family (mainly $LiNbO_3$, $LiTaO_3$ and $KTiOPO_4$) are commercially available, their IR transparency does not exceed 5 microns and therefore they cannot be used for deeper MIR applications. For instance the 8–14 μm range corresponding to one of the atmospheric transparency window is interesting for LIDAR or counter-measure systems while coherent sources in the strongly water-absorbing 6–7 μm range can be used for medical (surgery) applications. More generally tunable coherent MIR laser sources are useful spectroscopic tools to probe rovibrational molecular fingerprints with various applications in trace gas sensing such as environmental monitoring, detection of hazardous species, life science or medical applications such as real-time breath analysis for early disease diagnosis [1–5].

Currently very few nonlinear chalcogenide compounds possessing both wide transparency range above 5 μm and large energy bandgap are available. The bandgap wavelength requirement of $\lambda_g < 500$ nm is necessary to avoid two-photon absorption (TPA) when they are pumped with popular 1 μm range solid-state emitting lasers such as Nd^{3+} lasers or Yb^{3+} fiber lasers. Only a handful of ternary compounds satisfies the requirement of wide bandgap and extended MIR transparency range, with proven capabilities for down-conversion to the long-wave MIR ($\lambda > 5$ μm) using 1.064 μm pump optical parametric oscillation (OPO) [6]. Among these latter ones —whose use in nanosecond OPOs have been widely proven owing to their commercialization—one can quote the benchmark *wurzite*-type ternary chalcopyrite $AgGaS_2$ (AGS) belonging to the $A^{II}B^{IV}$ C_2^V semiconductor group and, to a lesser extent, the much more limited transparency range $ZnGeP_2$ (ZGP) belonging to the $A^{I}B^{III}$

C_2^{VI} group. During more than a decade silver gallium sulfide ($AgGaS_2$) has been the only OPO material with the longest demonstrated idler wavelength [7].

Since the mid 90's, some novel ternary lithium containing chalcogenides ($LiInS_2$, $LiInSe_2$, $LiGaS_2$, $LiGaSe_2$) produced with large enough single-crystal size have emerged [8, 9], leading to various nanosecond OPO demonstrations covering the mid-IR [10–12] despite their rather low nonlinearity ($d_{il} < 10$ pm V^{-1}) compared to ZGP or the difficult-to-grow mercury thiogallate, $HgGa_2S_4$ (HGS) [13, 14]. The recently re-discovered II–IV–V_2 chalcopyrite compound $CdSiP_2$ (CSP) with its high nonlinearity ($d_{36} = 92$ pm V^{-1} [6]) could appear as an alternative to ZGP, however its low bandgap ($\lambda_g \sim 539$ nm) combined with limited MIR transparence ($\lambda \leqslant 6.5$ μm) almost restrict its use to the non-critically phase-matched generation of ~6 μm radiation when pumped at 1064 nm [15]. Alternative to birefringence phase-matched compounds, orientation-patterned III-IV semi-conductors (orientation-patterned GaAs and GaP) with high nonlinearity have been recently engineered, however their low bandgap energy does not allow 1 μm pumping not only because of TPA but also due to strong absorption resulting in tremendous thermal load [16]. OP-GaAs and OP-GaP require thus pumping above ~2 microns and have limited aperture (<1 mm) due to quasi-phase-matching limitations [17, 18]. The continuous coverage of the MIR spectrum from 5 to 20 μm requires thus the continuous synthesis of novel nonlinear birefringent ternary chalcogenide compounds, combining both wide energy bandgap and extended MIR transmission.

Recently two new promising ternary chalcogenide compounds have been successfully synthesized in large size using the Bridgman-Stockbarger technique: $BaGa_4S_7$ (BGS) [19–21] and $BaGa_4Se_7$ (BGSe) [22, 23]. Both sulfide and selenide compounds exhibit wide bandgap energy ($E_g = 3.54$ eV with $\lambda_g = 0.350$ μm for BGS; $E_g = 2.64$ eV with $\lambda_g = 0.469$ μm for BGSe) and extended MIR transparency (up to 12 μm for BGS and from 0.47 to 18 μm for BGSe at 0% transparency level). The two compounds are biaxial, offering hence an extended phase-matching capability over their 0.3 cm^{-1} level transparency range (BGS: 0.545–9.4 μm; BGSe: 0.776–14.7 μm). However despite their similar chemical composition, BGS crystallizes in the *mm*2 orthorhombic point group as the isostructural $LiGaS_2$ while BGSe crystallizes in the monoclinic *m* point group (offering thus an extended phase-matching capability than BGS), with the dielectric axes *x* and *z* aligned respectively with the *b* and *c* crystallographic axes [21, 22]. Their nonlinear coefficients are however about twice smaller than that of $AgGaS_2$ ($d_{36} = 13$ pm V^{-1} [24]) but due to their largest bandgap both compounds exhibit much higher damage threshold at 1064 nm (1.2 J cm^{-2} for 12 ns pulse and 10 Hz repetition rate [19] and 3.7 J cm^{-2} for 14 ns pulse at 100 Hz [20]). The first BGS nanosecond OPO pumped by a Nd:YAG laser at 1064 nm was demonstrated by Tyazhev *et al* [25], in which the idler wave could be tuned from 5 to 7.3 μm, and delivering a maximum 0.5 mJ pulse energy at 6.2 μm. From this study and comparing with the performance of the 13× higher nonlinearity CSP compound in a similar OPO setup [6], the authors highlighted the advantage of the lower nonlinearity BGS stemming from of its 10× higher surface damage resistance compared with CSP.

The first BGSe nanosecond OPO ever reported was pumped by a Q-switched Ho:YAG laser at 2.09 μm and used a *y*-cut crystal ($\theta = 40.8°$, $\varphi = 0°$) for type-I (*o-ee*) phase-matching in the *xz* plane [26]. However the tunable 3–5 μm idler wavelength did not exceed the ~5 μm limit of oxide-based ferroelectrics and the down-conversion idler pulse energy (<1.4 mJ at 20 mJ pump) was quite modest despite the sample length used (dimension 6 × 6 × 30 mm^3). With a similarly cut but shorter BGSe sample (dimension 10.33 × 11.95 × 14.57 mm^3), a 1064-nm pumped BGSe OPO was reported in [27], demonstrating a considerably improved output performance in terms of both idler MIR tunability (2.7–17 μm) and output pulse energy (~3×). Using a wide pump beam diameter ($2w = 5$ mm) to accommodate for the available high-energy from the Nd:YAG laser (up to $E_p = 250$ mJ for 8 ns pulse at $f = 10$ Hz), 3.7 mJ at 7.2 μm from 63 mJ of pump pulse energy without any significant saturation in the observed 40% quantum conversion efficiency was obtained. This limitation was not due to the BGSe damage threshold but to that of the Au-coated OPO end mirror. As an important finding, the comparison of the nonlinear down-conversion efficiency of two samples, one phase-matched for type-I (*o-ee*) phase-matching in the *xz* dielectric plane ($d_{\text{eff}}(xz) = d_{16}\cos^2\theta + d_{23}\sin^2\theta$) and the other for type-II (*o-eo*) phase-matching in the *yz* plane ($d_{\text{eff}}(yz) = \pm d_{16}\cos\theta - d_{15}\sin\theta$), allowed to assess that the nonlinear tensor elements d_{16} and d_{23} must have the same sign [27].

In this article, we report on a $BaGa_4Se_7$ nanosecond OPO pumped for the first time by a Q-switched Nd:$YLiF_4$ (Nd:YLF) at 1053 nm, the shortest OPO pump wavelength used for this crystal. Contrary to [27], the pump laser has not only a slightly shorter wavelength but also much lower pulse energy (maximum energy 1.3 mJ). Low threshold of oscillation ($E_{\text{p,th}} = 0.25$ mJ) was achieved by reducing the pump beam diameter to $2w \sim 1$ mm, thus the reported performance corresponds to the operation of the OPO far below parametric gain saturation (and damage threshold). The MIR idler wave tunability extends from 2.6 μm to 10.4 μm, greater than for a mercury thiogallate (HGS) OPO pumped by the same Nd:YLF laser and employing an identical crystal length [14]. Despite the higher $\chi^{(2)}$ nonlinearity of HGS (4× that of BGSe), the idler output performance of our present BGSe OPO is 4 to 5 times higher than that of the HGS OPO, delivering a maximum pulse energy of 45 μJ

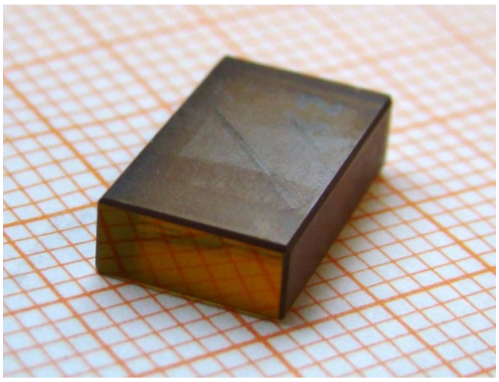

Figure 1. Photograph of the $BaGa_4Se_7$ sample. The darker yellow tinge results from some point defects absorption shoulder at the onset of the visible spectrum side.

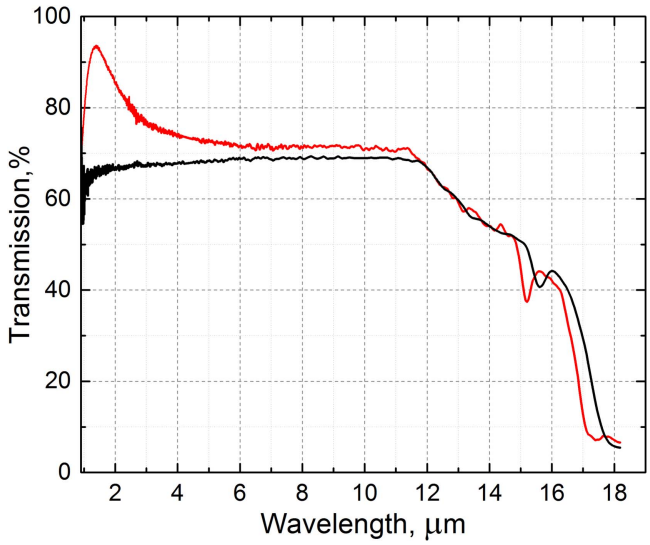

Figure 2. Unpolarized transmission spectra of the 11.8 mm $BaGa_4Se_7$ sample, before (black line) and after AR coating (red line), showing improved transmission at the pump and in the signal wave range (1.17–2.02 μm).

at ~3.3 μm and 14 μJ at ~8 μm, whereas the HGS OPO yielded less than 8 μJ over its whole tuning range (4.2–10.8 μm). We report on surface damage threshold measurements of BGSe at 1053 nm, confirming the high damage threshold (>2 J/cm^2 for 10 ns pulse and $f = 100$ Hz repetition rate) reported in [23] for similar experimental conditions. Additionally, with our phase-matched OPO data, we could infer the accuracy of three recently published dispersion and thermo-optic dispersion relations of $BaGa_4Se_7$.

2. Experimental nanosecond OPO set-up

The $BaGa_4Se_7$ optical element (dimensions $3 \times 7 \times 11.8$ mm^3, see in figure 1) used in this experiment was grown at High Technologies Laboratory, Kuban State University (Russia) using the Bridgeman–Stockbarger technique [20, 21]. It was cut for type-I (*o-ee*) phase-matching ($\theta = 45°$, $\varphi = 0°$) with the pump laser polarized ordinarily along the 3 mm side (direction of the *y*-dielectric axis) and the signal and idler waves polarized within the *xz* plane (top or bottom facet of the shown element in figure 1). The wider transverse aperture of 7 mm is designed to allow an extended angular tuning of the phase-matching. The crystal is maintained at a temperature of $T = 40$ °C(±0.1 °C) by means of a thermo-electric Peltier element. The crystal was single-layer anti-reflection (AR) coated at ~1.5 μm, resulting in a transmission greater than 85% over the bandwidth 1–2 μm as shown from FTIR spectrum (figure 2). The transmission in the mid-IR idler range (5–11 μm) is above 72%, slightly improved with respect to the uncoated sample transmission.

The experimental layout of the BGSe OPO is sketched in figure 3. The pump source is a diode-pumped Q-switched Nd:YLF laser (Laser-compact Group model TECH-1053-N). The pump wavelength is

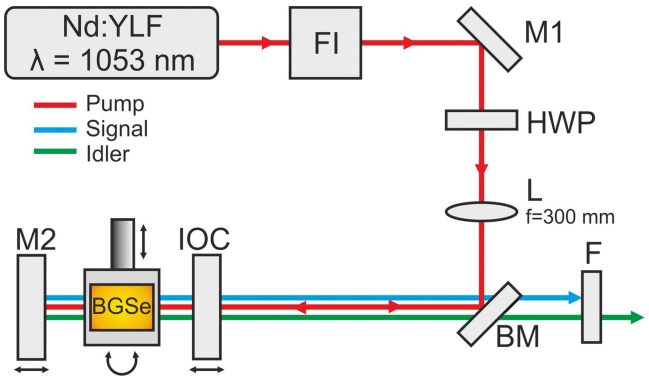

Figure 3. Experimental layout. HWP: Half-wave plate; BM: dichroic bending mirror; IOC: input-output ZnSe coupler; M2: gold mirror. F: interference filters for idler wave selection. The *xz* plane of BGSe is within the plane of the drawing.

$\lambda_p = 1.053$ μm and the pulse duration is $\tau = 16$ ns, with a pulse repetition rate set to $f = 100$ Hz. The specified bandwidth of the laser is ~1 cm^{-1} (30 GHz), within the pump acceptance bandwidth of the type-I phase-matching process. The maximum laser pulse energy is 1.3 mJ and the measured beam quality factors are $M_x^2 = M_y^2 = 1.3$. Due to the linear OPO cavity, the Q-switched Nd:YLF laser is protected from feedback radiation by a Faraday isolator (FI). A half-wave plate (HWP) is used to rotate the laser polarization vertically with respect to the *xz* plane of BGSe so as to satisfy the *o-ee* phase-matching requirement. Given the low pump pulse energy, in order to reach threshold of parametric oscillation, the pump beam diameter is reduced to a measured spot diameter of $2w_x = 0.84$ mm and $2w_y = 0.84$ mm by a $f = 300$ mm BK7 lens.

The pump pulses are directed to the linear OPO resonator by a 45° incidence ZnSe dichroic bending mirror (BM) which is HR-coated in a narrow 1.0–1.1 μm band (average reflectivity 97% at normal incidence) and highly transmitting ($T_{average} = 90\%$) from 1.15 μm to approximately 10 μm. Its use at 45° incidence results in further pump transmission leakage from the cavity. Several combinations of interference filters (F) were used to isolate as much as possible the idler wave from the pump and signal waves residual leakage from BM mirror.

The OPO cavity, configured as a double-pass pump, signal-resonant oscillator (SRO), is formed by the input-output ZnSe coupler (IOC) and a gold (Au) mirror M2 and the cavity length was kept as short as possible ($L_{cav} \geqslant 18$ mm) to increase the number of signal-wave roundtrips within the cavity so as to reduce the pump threshold. The IOC has a long radius of curvature $R = -1000$ mm so as to improve transverse signal beam confinement. Its transmission at $\lambda_p = 1.053$ μm is 93%. The IOC coupler was dielectrically coated so as to be reflecting for part of the entire signal wave band ($1.17 \leqslant \lambda_s \leqslant 2.155$ μm): Its reflectivity ranges from an average $R_s \approx 90\%$ from 1.28 μm to 1.8 μm and gradually decreases to $R_s \approx 60\%$ at 1.18 μm and 2.1 μm. Its average transmission is $T \sim 75\%$ in the idler range between 2.28 μm and 11 μm. Due to the narrow HR band of the bending mirror, most of the signal wave exiting IOC could leak through BM, and to separate the mid-IR idler from the leaking signal wave—especially for short idler wavelengths below $\lambda_i \approx 2.6$ μm—two dielectric mirror filters had to be used to minimize signal component contamination of the measured idler pulse energy. However these two high-pass filters could efficiently block only the signal wavelengths below ~1.683 μm, so that in the idler range from ~2.2 μm (near the $2\lambda_p$ degeneracy point) to 2.6 μm the idler pulse energy could not be properly measured due to strong signal contamination (thus only idler data from 2.6 μm have been plotted in figure 4). The idler energy was measured with a pyroelectric detector (OPHIR model VEGA PE10-C). To determine idler wavelength in spectral range from 2.6 μm to 10.4 μm the signal wavelength was measured by a commercial wavelength meter (*HighFinesse* models LSA L IR) and the idler wavelength was retrieved from energy conservation ($\lambda_p^{-1} = \lambda_s^{-1} + \lambda_i^{-1}$).

The BGSe sample was hold inside a copper mount that is temperature-regulated at $T = 40$ °C by means of a thermo-electric Peltier element. For wavelength tuning purpose, the BGSe mount is positioned on a motorized high-precision rotation mount (STANDA model 8-MR-191-30) for the calibration of the internal θ phase-matching angle (deduced from the external incidence angle using Snell's law). The rotation stage itself is mounted on a motorized X-translation stage (STANDA model 8MT173-20), which automatically adjust the lateral position of the BGSe crystal respective to the cavity axis as the crystal is rotated. A PC controller monitored the θ—position and X-lateral position of the crystal. To accommodate rotational tuning of the phase-matching (the BGSe cut angle $\theta = 45°$ corresponds to an idler wavelength of $\lambda_i \approx 8$ μm), the cavity length was increased by linear translation of mirror M2 and IOC.

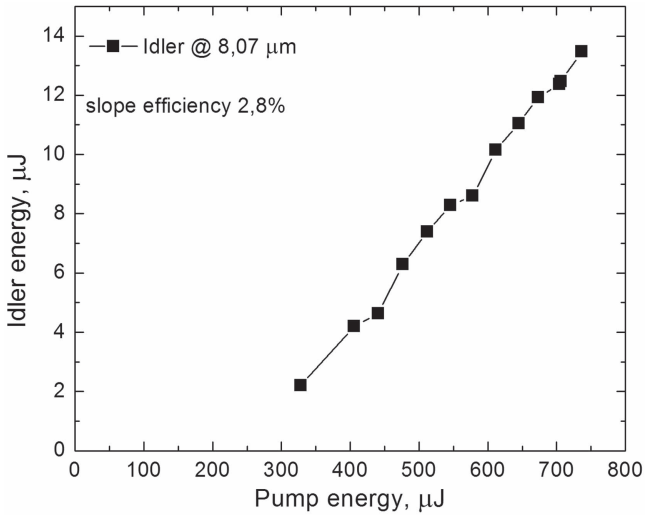

Figure 4. $BaGa_4Se_7$ nanosecond OPO measured idler energy at ~8 μm versus pump pulse energy measured in front of the OPO cavity (after BM). The idler energy was the net energy measured just after the BM mirror (hence corrected for transmission loss due to BM and the two additional filters, but not for the transmission of IOC).

3. Experimental results: conversion efficiency and mid-infrared tuning

Figure 4 shows the BGSe OPO idler pulse energy at $\lambda_i = 8.07$ μm (corresponding to sample at normal incidence and a short cavity length $L_{cav} = 18$ mm) as the pump pulse energy is increased.

At this idler wavelength, $\lambda_s = 1.211$ μm with a IOC reflectivity $R_s = 70\%$. The threshold pump energy is extrapolated to be $E_{p,th} = 250$ μJ. This threshold is about 25× lower than that reported in the previous BGSe-OPO employing a 5× larger pump beam diameter [27]. The intensity threshold of a singly-resonant, critically phase-matched, nanosecond OPO can be expressed as [28, 29],

$$I_{th} = \frac{1.8}{\kappa g_s L_{\text{eff}}^2 (1+\gamma)^2}\left(\frac{25 L_{\text{cav}}}{c\tau} + 2\alpha l_c + \ln\frac{1}{\sqrt{R}} + \ln 2\right)^2 \quad (1)$$

In equation (1), $\kappa = 2\omega_s\omega_i d_{\text{eff}}^2/n_s n_i n_p \epsilon_0 c^3$ is the nonlinear coupling constant; $g_s = w_p^2/(w_p^2 + w_s^2)$ is the mode-coupling coefficient (g_s~0.465 in our case assuming equal confocal parameter for the resonating signal and the pump); $l_c = 11.8$ mm is the crystal length; $L_{\text{eff}} < l_c$ is an effective parametric gain length [29] taking into account the walkoff angle of the extraordinary signal wave ($\rho_s = 2.62$ mrad $= 1.7°$); L_{cav} is the cavity length; $\alpha \approx 0.05$/cm is the signal absorption coefficient; $\tau = 16$ ns is the pump pulse width. The coefficient γ is the ratio of the forward and backward pump amplitude ($\gamma \sim 1$ in our double-pump pass SRO) and $R = R_{\text{in}} R_{\text{out}} (1 - R_c)^4$ is an overall reflectivity coefficient for a round-trip cavity (for an AR-coated sample, and $R_{\text{in}} = R_{\text{out}} \sim 0.9$ is the IOC coupler reflectivity for the signal wave). In our case, given the uncertainties on those parameters, one can estimate $0.5 \leqslant R \leqslant 0.8$. Computing the effective parametric gain length yields $L_{\text{eff}} \sim 0.9 l_c$.

A direct evaluation of the threshold from (1) would require the knowledge of $d_{\text{eff}} = d_{16}\cos^2\theta + d_{23}\sin^2\theta \approx 0.5(d_{23} + d_{16})$ at $\theta = 45$ deg. However only d_{23} is currently known (its value at $\lambda_i = 9$ μm was measured to be 10.5 ± 0.5 pm V^{-1} in [30]). The magnitude and relative sign of d_{16} are still unknown, and in [27] the authors have been led to conclude that both nonlinear tensor elements should have the same sign. In order to get an insight on this issue, we use equation (1) to derive an estimation of the effective d_{eff} by comparing the theoretical threshold to the one we have experimentally measured ($E_{p,th} = 0.25$ mJ resulting in $I_{p,th} = 2.75$ MW cm^{-2} for $w_p = 0.42$ mm). Depending of the chosen values of R in the above uncertainty range, extracting the value of the effective nonlinear coefficient from equation (1) leads to 12 pm V$^{-1} \leqslant d_{\text{eff}} \leqslant 22$ pm V^{-1}. Because $d_{\text{eff}} = 0.5(d_{23} + d_{16})$ for $\theta = 45°$, this rough and indirect estimation pledges for both nonlinear tensor elements to have the same sign, given that $d_{23} \approx 10$ pm/V, as already pointed out in [27] from the comparison of the performance of type-I versus type-II BGSe OPOs. Assuming different signs for d_{16} and d_{23} would result in a much lower d_{eff} outside the boundaries reported above. A direct measurement of the relative sign and magnitude of d_{16} remains thus necessary.

Turning back to figure 4, the maximum idler energy at 8.07 μm (~14 μJ) was limited by the available Nd:YLF pulse energy. The data could be excellently fitted with a straight line, showing no sign of saturation as expected since the BGSe OPO is pumped even farther from parametric gain saturation as done in [27] that used up to 63

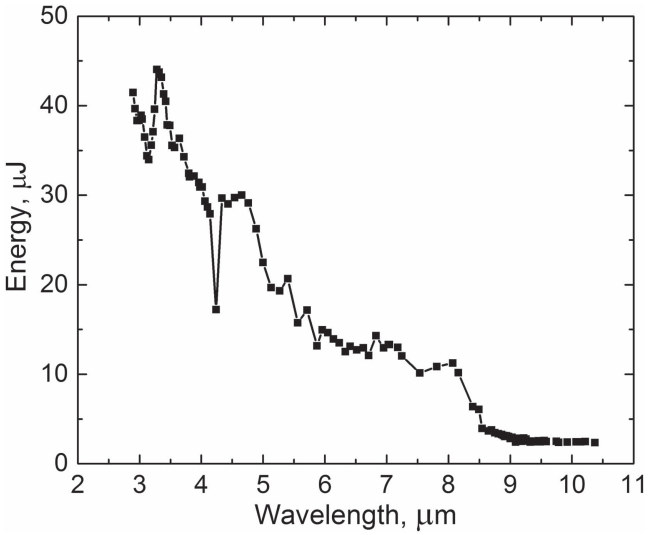

Figure 5. Plot of idler pulse energy versus idler wavelength.

mJ of Nd:YAG pumping with a much larger beam diameter ($2w = 5$ mm) to avoid damage. Comparing with the performance of a ns OPO pumped with the same Nd:YLF laser and employing a similar length mercury thiogallate (HGS cut for type-II eoe at $\theta = 47°$; $\varphi = 0°$ with $d_{eff} \cong d_{36}$), and which yielded 2 μJ of idler at $\lambda_i = 7.5$ μm (normal incidence) [14], the performance of this BGSe OPO is about 7× superior despite the 4× superior value of HGS effective nonlinear coefficient. Because the OPO mirror cavity reflectivities were almost comparable, this difference in performance may be mainly attributed to the superior optical quality of $BaGa_4Se_7$ with respect to $HgGa_2S_4$ whose growth in large size, good quality is extremely difficult. Furthermore with its larger energy bandgap ($E_g = 2.79$ eV instead of 2.64 eV for BGSe [6]) one would have expected a better performance for the HGS OPO. The measured $s = 2.8\%$ energy slope efficiency in figure 4 corresponds to $q = s(\lambda_i/\lambda_p) = 21\%$ quantum conversion efficiency, far from pump saturation and back-conversion.

Figure 5 displays the idler energy measured after IOC mirror as a function of wavelength. For reasons explained in the previous section, we did not plot the data below $\lambda_i = 2.6$ μm down to 2.2 μm because of imperfect separation of the idler energy from the leaking signal energy. The MIR coverage (2.2–10.5 μm) obtained with a single BGSe crystal exceeds the one (5.6–10.8 μm) obtained from the previously quoted HGS OPO, that needed two samples ($\theta = 47°$ and at $\theta = 60°$) to cover that idler range [14]. This broad coverage with a single sample highlights the broader phase-matching capability of the monoclinic $BaGa_4S_7$ compared with the uniaxial defect chalcopyrite $HgGa_2S_4$. The general decreasing trend of the OPO performance in figure 5 relates to the λ_i^{-1} dependence of the parametric gain. The OPO could deliver a maximum of 50 μJ of idler energy at ~3.3 μm ($\lambda_s = 1.55$ μm). The peak around 3.3 μm coincides with an OPO configuration where the IOC reflectivity is $R_s \geqslant 95\%$ between 1.4 μm and 1.62 μm. The dip at 4.2 μm and those in the 5.5–6 μm range are probably due to atmospheric absorbing molecular species (such as water). The slight enhancement bump centered at 8.1 μm corresponds to the usually observed enhancement of such nanosecond OPOs when the crystal is phase-matched at normal incidence with respect to the linear cavity axis [25, 27], resulting in a sub-cavity etalon effect originating from the plane parallel crystal facets that are uncoated for the idler wave. Compared to [27], the magnitude of the bump is weaker due to the 10× reduced diameter or the pump beam.

As to the *plateau* behavior between 9.2 and 10.4 μm, it corresponds to signal wavelengths for with the reflectivity of the IOC coupler drops severely between $R = 20\%$ and 50%. The much weaker signal wave resonance probably prevents a genuine parametric oscillation, giving rise rather to an *amplified* parametric generation.

The phase-matching angles associated with the MIR tuning curve shown in figure 5 are plotted in figure 6.

As seen the OPO idler wave could be tuned from nearly the degeneracy point ($\lambda_s = \lambda_i = 2\lambda_p = 2.106$ μm) to 10.5 μm. Actually the near-IR wavelength meter could measure directly the lower wavelength part of the idler branch (plotted with filled circle symbol) while the MIR part was deduced by measuring the signal wave (filled square symbol) and making use of pump photon energy conservation. For obvious reasons due to the limited pump pulse power of the Nd:YLF laser ($E_p < 1$ mJ at the OPO) combined with decreasing parametric gain (resulting in higher threshold), we could not achieve the largest ever reported MIR tuning in [27]—up to 17 μm —obtained with a similar BGSe sample but a high-power Nd:YAG pump laser ($E_p > 100$ mJ).

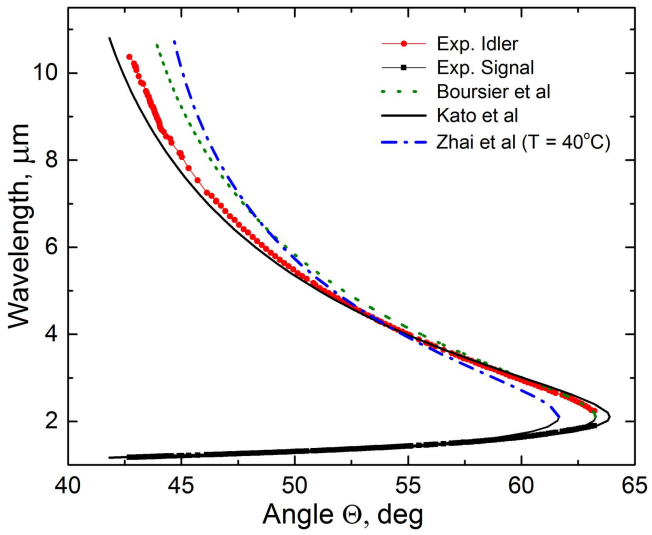

Figure 6. Nd:YLF pumped ($\lambda_p = 1.053$ μm) type-I (*o-ee*) $BaGa_4S_7$ OPO phase-matching tuning curve.

Very recently new dispersion formulae (Sellmeier equations) for BGSe have been proposed by three different groups [31–33], and their accuracy has been tested with our experimental phase-matching data taken at relatively low pump power, i.e. without any self-heating bias (due to residual absorption) introduced by high-power phase-matched data. In [32] thermo-optic Sellmeier equations for the three principal dielectric axis of BGSe were constructed for the first time, using direct index of refraction measurements of prisms maintained at some fixed temperatures spanning 25–150 °C and employing the minimum deviation angle technique to derive the index of refraction. Mercury, Helium and Cadmium lamp lines between 0.546 μm and 2.325 μm were used for the temperature-dependent index measurement at a relative accuracy level of a few parts in 10^{-4}. The authors worked out temperature-dependent Sellmeier equations which yield the (blue) dash-dot curve labelled 'Zhai *et al* (T = 40 °C)'. Large deviation from the measured experimental data can be observed not only near the degeneracy turning point but also at long-wave idler above 4 μm. Setting the temperature to $T = 25$ °C would lead to an even larger discrepancy of Zhai's equations for long wave MIR. Such large discrepancies find their origins in the customary inability of direct index measurements—even at the 10^{-4} relative accuracy—to reflect experimental phase-matched data at less than a few degrees. Another origin of the inaccuracy of the Sellmeier data proposed in [32] is the limited MIR wavelength range of their index measurements (the longest wavelength being 2.325 μm).

The second set of Sellmeier equations (at room temperature), obtained by refinement of the two-pole Sellmeier equations in [21], that we used to model our experimental phase-matched data are taken from [31]. The authors used phase-matched difference-frequency generation (DFG) data extending down to 11 μm to propose refined dispersion relations for BGSe. The theoretical curve based on their Sellmeier equations is plotted with dot (green) line in figure 6. While these dispersion relations account fairly well our experimental data near the degeneracy turning point, they fail to account for experimental idler wavelength data above ~4 μm again, despite the fact that the DFG data used in [31] extended to 11 μm. The same discrepancy for idler wavelengths >4 μm was also noted in the Nd:YAG laser pumped BGSe OPO in [27].

Finally the most accurate Sellmeier equations that reproduce fairly well our entire OPO phase-matched dataset is the ones worked out by Kato *et al* at room temperature [33]. Kato *et al* worked out their dispersion relations from second-harmonic generation (SHG) of the signal/idler components of a 1.064 μm pumped $AgGaS_2$ OPO, supplemented with data from phase-matched sum frequency generation (SFG) of a CO_2 laser (10.59 μm) and the signal/idler wave from the AGS OPO. The calculated curve based on their refined two-pole Sellmeier equations is plotted with solid(black)-line in figure 6. We infer the relatively fair accuracy of their dispersion relations to the fact that they were based on a rather dense wavelength set spanning the whole 1–11 μm range.

The pulse duration of the pump, signal, and idler waves were also investigated. Figure 7 shows the temporal traces of the incoming pump pulse, and output signal and idler pulses. The pump and signal pulses were detected with a fast InGaAs photodetector (Thorlabs Inc. model FGA-04) while the MIR idler pulse was monitored with a fast Mercury Cadmium Telluride (HgCdTe) photodetector having a response time less than 1.5 ns (VIGO Systems model PVM-10.6). All temporal signals were displayed on a 2.5 GHz bandwidth oscilloscope (LeCroy Wavesurfer 62XS). Unlike in the high-depletion Nd:YAG pumped OPO described in [27] for which the signal

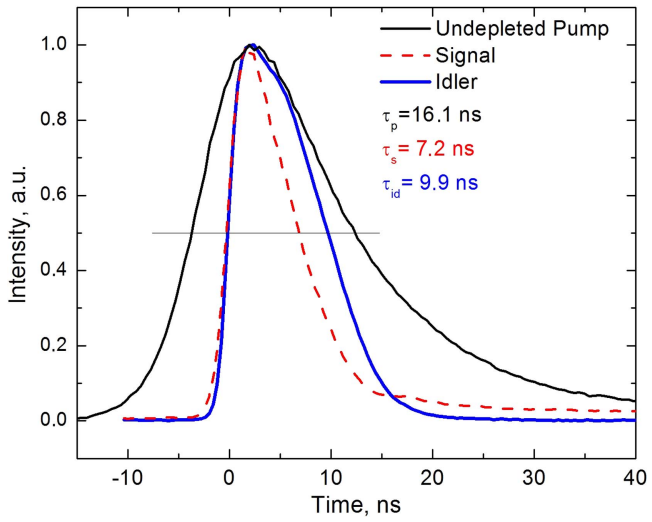

Figure 7. Comparison of the input pump pulse with the output signal and idler wave pulses. The duration values given in the inset refers to FWHM pulse duration.

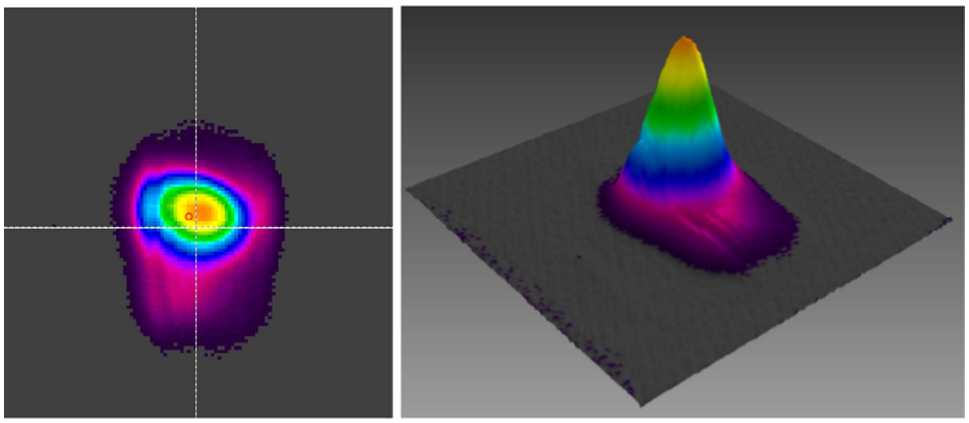

(a) (b)

Figure 8. The measured 2D (a) and 3D (b) idler beam profile.

build-up time was shorter, in our low power experiment this build-up time is slightly longer. Also the idler FWHM pulse width was found to be shorter than the pump pulse width contrary to [27], in agreement with the linear regime of conversion efficiency shown in figure 4.

4. The beam profile and M^2 measurements

Figure 8 represents the 2D (a) contour plot and 3D profile (b) of the mid IR idler beam profile at 7.6 μm, measured with a commercial infrared Spiricon PYROCAM-III camera equipped with $LiTaO_3$ pyroelectric detector (active area, 12.4 $\times$ 12.4 mm; element size, 0.1 $\times$ 0.1 mm). The Si lens with focal length 100 mm was used for the measurement of beam widths as function of propagation distance. The M^2 measurement was carried out at the following conditions: $E_{pump} = 670\ \mu J$, $f = 1000$ Hz. As can be noticed the idler beam profile is far from a Gaussian pattern as often expected for nanosecond OPOs, exhibiting in particular a pedestal in the vertical direction. A software automatically evaluates the beam diameter at $1/e^2$ intensity level. For the plot in figure 9, the distance between the lens and the camera was varied from 13.5 cm to 36.5 cm.

The plot in figure 9 displays the experimental values of square of the beam width D_g in terms of Gaussian approximation, both along the horizontal (black squares) and vertical (red bold circles) transverse directions. The fitting of the squared widths with a quadratic polynomial was made according to international standard ISO 11146-1-2005. The resulting M^2 factors obtained from the fits are $M_x^2 = 24$ and $M_y^2 = 20$ for the idler beam at $\lambda = 7.6\ \mu$m. Compared to the previous high-energy, high-efficiency BGSe OPO experiments reported in [27],

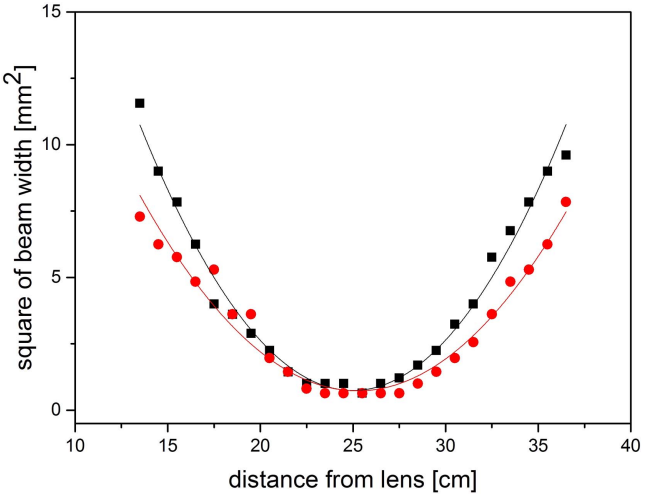

Figure 9. Experimental values of square of beam widths in terms of Gaussian approximation.

these M^2 values are however smaller (values as large as $M_x^2 = 40$ and $M_y^2 = 60$ were then reported, due to back-conversion distortions and the large Fresnel number cavity.

5. Damage threshold measurements

Damage threshold of MIR nonlinear materials are key parameters for high-power laser applications. Owing to its large bandgap, $BaGa_4Se_7$ displays ~4× higher surface damage threshold than the ternary chalcopyrite such as $AgGaS_2$ or $AgGaSe_2$ [22]. Damage thresholds for low repetition rate pulse are usually expressed in terms of energy fluence F (in unit of J/cm^2) while in high repetition rate regime or continuous-wave, they can be expressed in terms of intensity (in unit of W/cm^2). The first damage thresholds measurements on $BaGa_4Se_7$, performed with 1.064 μm pulses ($\tau = 5$ ns, $f = 1$ Hz) focused to $2w = 0.4$ mm beam diameter, have been previously reported and yielded $F_{th} = 2.8$ J cm^{-2} (corresponding to an intensity $I_{th} = 557$ MW cm^{-2}) [22]. But since damage may also depend on crystal quality it is worth measuring it with respect to the higher quality sample of the same origin used in [27], for which a twice lower surface damage threshold of $F_{th} = 1.4$ J cm^{-2} ($\tau = 14$ ns, $f = 100$ Hz, $2w = 5$ mm) has been estimated. This fluence translates to $I_{th} = 100$ MW cm^{-2} which is the highest damage threshold value among non-oxide MIR nonlinear compounds, except for $LiGaS_2$ and $BaGa_4S_2$ (BGS) having even larger bandgap than BGSe. The twice smaller damage threshold measured by the authors of [27] was attributed to the 10× larger beam diameter they used compared to the 0.5 mm diameter used in [22]. Indeed sampling larger surface addresses more local surface defects or impurities.

In order to characterize the damage threshold of our sample, several thin (~1–2 mm) plates cut with the same orientation and from the same ingot as the present OPO sample were prepared and polished. Some of them were AR coated as the OPO sample, but these AR-coated test plates definitely displayed twice lower damage threshold than the uncoated ones, meaning that the damage observed relates rather to the dielectric ARC layer. In the following we report thus only on damage of uncoated samples. In order to increase the energy fluence of the Nd:YLF laser (with maximum pulse energy 1.3 mJ in a $M^2 < 1.3$ beam quality factor and a pulse duration $\tau = 16$ ns) the laser beam was focused down to a diameter $2w = 200$ μm and the surface of each sample was mapped every mm^2 and scanned with the focused beam. Each mapped area was exposed during 5 min and the sample surface was examined after each exposure with a microscope in order to identify eventual dark spots. The pulse energy fluence is then incremented in steps of 0.05 J/cm^{2}and the process repeated until trace of dark (burned) spots appear under microscope examination. The damage fluence threshold is defined as the fluence just preceding the observation of these *surface* dark spots. We studied the damage formation at 3 repetition rate values of the Q-switched laser: $f = 100$, 150 and 200 Hz.

Figure 10(a) shows the picture of one of the test plates after irradiation, displaying a constellation of faint and much darker and larger spots, the latter ones appearing beyond the defined threshold fluence (just after observation of the faint spots). As the laser pulse energy is increased, the larger surface spots develop as craters inside the material. On much thinner samples—that had to be fixed on a metal holder with a ring aperture—these craters may even evolve into a crack, fracturing the sample. Such a crack is highlighted by the white vertical arrow in figure 10(b).

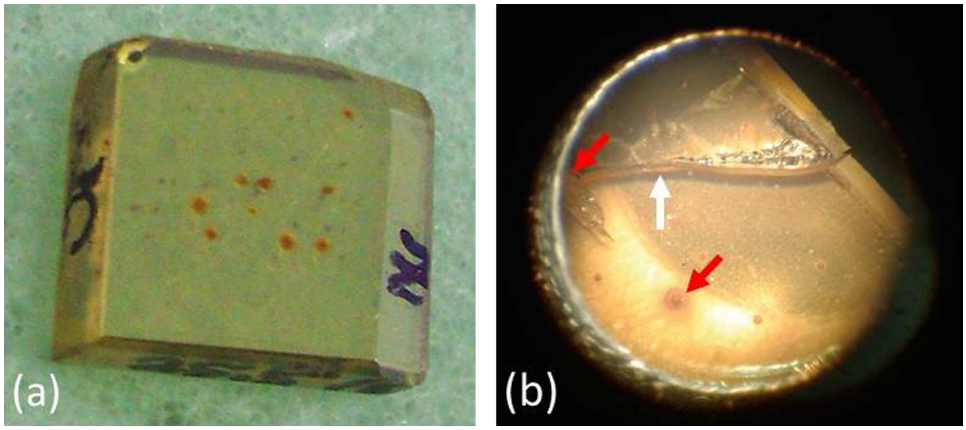

Figure 10. (a) Uncoated $BaGa_4Se_7$ plate showing the formation of surface dark damage spots of increasing size as the Nd:YLF laser pulse fluence is increased above the damage fluence threshold; (b) Thinner sample as seen through the circular hole of its metallic holder: As the fluence is further increased, craters are formed at the dark spots locations (red arrows) and may even induce a crack trail (white vertical arrow).

Table 1. Result of energy fluence and intensity surface damage threshold measurements in $BaGa_4Se_7$ test samples irradiated by the Q-switched Nd:YLF pulses ($\tau = 16$ ns) at 1.053 μm with a beam diameter $2w = 200$ μm.

f_{rep} (Hz)	F_{th} (J cm^{-2})	I_{th} (MW cm^{-2})	Peak on-axis I_{th}(MW cm^{-2})
100	2.04 ± 0.39	127.3 ± 24.1	254.6
150	2.02 ± 0.31	126.0 ± 19.6	252
200	1.81 ± 0.25	112.8 ± 15.7	225.6

The final results of the damage threshold measurements are summarized in table 1, each row representing a fixed repetition rate of the Nd:YLF laser. The damage threshold F_{th} and I_{th} refer to an average irradiated area πw^2 while the last column is the peak on-axis intensity threshold defined as $2 \times I_{th}$. From the table it can be seen that the onset of damage threshold diminishes as the pulse repetition rate is increased. The decrease is relatively modest (~1%) from $f = 100$ to 150 Hz so that the damage threshold can be considered as constant up to 150 Hz, but an abrupt decreasing trend is noted at $f = 200$ Hz (~11%). Extrapolation of our data to $f = 1$ Hz as in [22] is not straightforward, but our value $F_{th} \sim 2$ J/cm^2 is rather consistent with the value 2.8 J/cm^{2}given in this reference at $f = 1$ Hz, $\tau = 5$ ns and $\lambda = 1.064$ μm. These values, related to small beam diameters, are among the highest for a mid-IR nonlinear crystal and confirm the beam diameter-dependent threshold value hinted in [27].

6. Concluding remarks

We have demonstrated a low threshold $BaGa_4Se_7$ nanosecond optical parametric oscillator pumped for the first time by a Q-witched Nd:$YLiF_4$ low power laser at 1.053 μm. With less than 1 mJ pump pulse energy, the OPO threshold was as low as 250 μJ at an idler wavelength of 8.1 μm. The comparison of this experimental threshold with theory allowed us to estimate a nonlinear effective coefficient (for type-I (o-ee) down-conversion in the xz plane) exceeding 12 pm V^{-1}. Such a large value seems to indicate that the relative sign of the d_{23} and d_{16} tensor elements of $BaGa_4Se_7$ should be the same. A maximum idler energy up to 45 μJ at 3.3 μm and 14 μJ at 8.1 μm has been achieved. A wide mid-IR idler wave coverage of 2.6–10.5 μm has been obtained using a single type-I cut crystal, confirming the promising status of this newly discovered biaxial monoclinic chalcogenide compounds for efficient mid-IR nonlinear down-conversion over its full transparency range (0.47–18 μm). Our down-conversion phase-matching angle measurements were further compared with recently constructed linear dispersion relations for this material, with a good agreement found with the Sellmeier equations of Kato *et al* [33]. Finally our damage threshold measurements (~2 J/cm^2 at 100 Hz repetition rate) are found in fair agreement with a previous measurement performed at 1.064 μm by another group [23] at similar beam diameter conditions.

Acknowledgments

This research has received funding from program NSU 5-100 of Russian Ministry of Science and Education. We acknowledge also support from 'Special Technology LTD' (Novosibirsk). J-J Zondy acknowledges the support from a Nazarbaev University ORAU research grant (No 064.01.01.SST2017032).

ORCID iDs

D B Kolker https://orcid.org/0000-0002-6325-6391

References

[1] Tittel F, Richter D and Fried A 2003 Mid-infrared laser applications in spectroscopy *Solid-State Mid-Infrared Laser Sources* Topics Appl. Phys. 89 ed I T Sorokina and K L Vodopyanov (Berlin Heidelberg: Springer) 2003 pp 445–516
[2] Sigrist M W 2000 Mid-infrared laser-spectroscopic sensing of chemical species *J. Adv. Res.* **6** 529–33
[3] Yu E M and Yu R M 2013 On the potential of mid-IR lasers for generating high harmonics with subnanometer wavelengths in gases *Quantum Electron.* **43** 211–6
[4] Le A T, Wei H, Jin C and Lin C D 2016 Strong-field approximation and its extension for high-order harmonic generation with mid-infrared lasers *J. Phys. B: At. Mol. Opt. Phys.* **49** 053001
[5] Le A T, Wei H, Jin C, Tuoc V N, Morishita T and Lin C D 2014 Universality of returning electron wave packet in high-order harmonic generation with midinfrared laser pulses *Phys. Rev. Lett.* **113** 033001
[6] Petrov V 2015 Frequency down-conversion of solid-state laser sources to the mid-infrared spectral range using non-oxide nonlinear crystals *Prog. Quantum Electron.* **42** 1–106
[7] Vodopyanov K L, Maffetone J P, Zwieback I and Ruderman W 1999 $AgGaS_2$ optical parametric oscillator continuously tunable from 3.9 to 11.3 μm *Appl. Phys. Lett.* **75** 1204
[8] Fossier S *et al* 2004 Optical, vibrational, thermal, electrical, damage and phase-matching properties of lithium thioindate *J. Opt. Soc. Am.* B **21** 1981–2007
[9] Petrov V *et al* 2010 Optical, thermal, electrical, damage, and phasematching properties of lithium selenoindate *J. Opt. Soc. Am.* B **27** 1902–27
[10] Zondy J J, Vedenyapin V, Yelisseyev A, Lobanov S, Isaenko L and Petrov V 2005 $LiInSe_2$ nanosecond optical parametric oscillator *Opt. Lett.* **30** 2460
[11] Tyazhev A, Vedenyapin V, Marchev G, Isaenko L, Kolker D, Lobanov S, Petrov V, Yelisseyev A, Starikova M and Zondy J J 2013 Singly-resonant optical parametric oscillation based on the wide band-gap mid-IR nonlinear optical crystal $LiGaS_2$ *Opt. Materials* **35** 1612–5
[12] Vedenyapin V, Boyko A, Kolker D, Isaenko L, Lobanov S, Kostyukova N, Yelisseyev A, Zondy J J and Petrov V 2016 $LiGaSe_2$ optical parametric oscillator pumped by a Q-switched Nd:YAG laser *Laser Phys. Lett.* **13** 115401
[13] Badikov V V, Don A K, Mitin K V, Seregin A M, Sinaiskii V and Vand Shchebetova N I 2003 A $HgGa_2S_4$ optical parametric oscillator *Quantum Electron.* **33** 831
[14] Kostyukova N Y, Kolker D B, Zenov K G, Boyko A A, Starikova M K, Sherstov I V and Karapuzikov A A 2015 Mercury thiogallate nanosecond optical parametric oscillator continuously tunable from 4.2 to 10.8 μm *Laser Phys. Lett.* **12** 095401
[15] Petrov V, Schunemann P G, Zawilski K T and Pollak T M 2009 Noncritical singly resonant optical parametric oscillator operation near 6.2 μm based on a $CdSiP_2$ crystal pumped at 1064 nm *Opt. Lett.* **34** 2399
[16] Insero G, Clivati C, D'Ambrosio D, De Natale P, Santambrogio G, Schunemann P G, Zondy J J and Borri S 2016 Difference frequency generation in themid-infrared with orientation-patternedgallium phosphide crystals *Opt. Lett.* **41** 5114–7
[17] Leindecker N, Marandi A, Byer R L, Vodopyanov K L, Jiang J, Hartl I, Fermann M and Schunemann P G 2012 Octave-spanning ultrafast OPO with 2.6–6.1 μm instantaneous bandwidth pumped by femtosecond Tm-fiber laser *Opt. Express* **20** 7046
[18] Schunemann P G, Pomeranz L A and Magarrell D J 2015 First OPO based on orientation-patterned gallium phosphide (OP-GaP) 2015 *CLEO 2015 Digest, Paper* SW3O.1 (Optical Society of America, 2015)
[19] Lin X, Zhang G and Ye N 2009 Growth and characterization of $BaGa_4S_7$: a new crystal for mid-IR nonlinear optics *Crystal Growth & Design* **9** 1186–9
[20] Guo Y, Zhou Y, Lin X, Chen W and Ye N 2014 Growth and characterizations of $BaGa_4S_7$ crystal *Opt. Materials* **36** 2007–11
[21] Badikov V, Badikov D, Shevyrdyaeva G, Tyazhev A, Marchev G, Panyutin V, Noack F, Petrov V and Kwasniewski A 2011 $BaGa_4S_7$: wide-bandgap phase-matchable nonlinear crystal for the mid-infrared *Opt. Mat. Express* **1** 316–20
[22] Badikov V, Badikov D, Shevyrdyaeva G, Tyazhev A, Marchev G, Panyutin V, Petrov V and Kwasniewski A 2011 Phase-matching properties of $BaGa_4S_7$ and $BaGa_4Se_7$: wide-bandgap nonlinear crystals for the mid-infrared *Phys Status Solidi RRL* **5** 31–3
[23] Yao J, Yin W, Feng K, Li X, Mei D, Lu Q, Ni Y, Zhang Z, Hu Z and Wu Y 2012 Growth and characterization of $BaGa_4Se_7$ crystal *J. Cryst. Growth* **346** 1–4
[24] Zondy J J, Touahri D and Acef O 1997 Absolute value of the d_{36} nonlinear coefficient of $AgGaS_2$: prospect for a low-threshold doubly resonant oscillator-based 3:1 frequency divider *J. Opt. Soc. Am.* B **14** 2481–97
[25] Tyazhev A, Kolker D, Marchev G, Badikov V, Badikov D, Shevyrdyaeva G, Panyutin V and Petrov V 2012 Midinfrared optical parametric oscillator based on the wide-bandgap $BaGa_4S_7$ nonlinear crystal *Opt. Lett.* **37** 4146–8
[26] Yuan J H, Li C, Yao B Q, Yao J Y, Duan X M, Li Y Y, Shen Y J, Wu Y C, Cui Z and Dai T Y 2016 High power, tunable mid-infrared $BaGa_4Se_7$ optical parametric oscillator pumped by a 2.1 μm Ho:YAG laser *Opt. Express* **24** 6083–7
[27] Kostyukova N, Boyko A, Badikov V, Badikov D, Shevyrdyaeva G, Panyutin V, Marchev G, Kolker D and Petrov V 2016 Widely tunable in the mid-IR $BaGa_4Se_7$ optical parametric oscillator pumped at 1064 nm *Opt. Lett.* **41** 3667
[28] Hellström J, Pasiskevicius V, Laurell F and Karlsson H 1999 Efficient nanosecond optical parametric oscillators based on periodically poled KTP emitting in the 1.8–2.5 μm spectral region *Opt. Lett.* **24** 1233–5
[29] Brosnan S J and Byer R L 1979 Optical parametric oscillator threshold and linewidth studies *IEEE J. Quantum Electron.* QE- **15** 415
[30] Boursier E, Seconds P, Debray J, Inacio P L, Panyutin V, Badikov V, Badikov D, Petrov V and Boulanger B 2015 Angle noncritical phase-matched second-harmonic generation in the monoclinic crystal $BaGa_4Se_7$ *Opt. Lett.* **40** 4591

[31] Boursier E, Seconds P, Ménaert B, Badikov V, Panyutin V, Badikov D, Petrov V and Boulanger B 2016 Phase-matching directions and refined Sellmeier equations of the monoclinic acentric crystal $BaGa_4Se_7$ *Opt. Lett.* **41** 2731
[32] Zhai N, Li C, Xu B, Bai L, Yao J, Zhang G, Hu Z and Wu Y 2017 Temperature-dependent sellmeier equations of IR nonlinear optical crystal $BaGa_4Se_7$ *Crystals* **7** 62
[33] Kato K, Miyata K and Petrov V 2017 Phase-matching properties of $BaGa_4Se_7$ for SHGand SFG in the 0.901–10.5910 μm range *Appl. Opt.* **56** 2978